ChemComm

Water-Soluble Endohedral Metallofullerenes: New Horizons for Biomedical Applications

SCHOLARONE™
Manuscripts

ChemComm

ARTICLE

Water-Soluble Endohedral Metallofullerenes: New Horizons for Biomedical Applications

William P. Kopcha,[a] Rohin Biswas,[a] Yue Sun,[a] Sy-Tsong Dean Chueng,[b] Harry C. Dorn, [c*] and Jianyuan Zhang [a*]

Endohedral metallofullerenes (EMFs) offer a safe avenue to manipulate metals important to biomedical applications such as MRI contrast, X-ray contrast, radiolabeling, radiotherapy, chemotherapy, and the control of inflammation by scavenging reactive oxygen species (ROS). Moreover, functionalizing the double bonds on the surface of EMFs modifies their solubility, supramolecular behaviour, binding, targeting characteristics, and physical properties. While most existing water-soluble derivatives possess a statistical mixture of appended functional groups, progress has been made in creating molecularly-precise derivatives with a defined number of surface functional groups, leading to potentially more nuanced control of their behaviour and properties. Further elucidation of the structure-function relationships of these materials is expected to enhance their utility in biomedical applications and possibly broaden their use in diverse areas of science and technology.

Introduction

For several decades, water-soluble metal salts and complexes have played a critical role in the realm of biomedical applications. Beyond their successful deployment as independent therapeutic agents, notably in chemotherapy[1,2] and brachytherapy,[3] they have demonstrated exceptional utility in imaging. The combination of their heavy nuclei, robust magnetic properties, and radioactivity has facilitated their application as contrast agents for computed tomography (CT),[4,5] magnetic resonance imaging (MRI),[6,7], and positron emission tomography (PET)[8,9]. This has empowered medical practitioners to enhance visualization, improve diagnosis, and refine treatment strategies, ultimately contributing to a superior standard of patient care.

While the utility and efficacy of metal-based therapeutic and diagnostic agents have been a great boon to modern medicine, researchers continually seek to increase efficacy and reduce associated side effects. For instance, gadolinium chelates, despite their successful application as MRI contrast agents, have been associated with nephrogenic systemic fibrosis (NSF)[7,10,11] as well as gadolinium deposition in the brain[12,13] due to heavy metal leakage from the chelation complex, presenting a notable area of opportunity for MRI contrast agents that do not suffer from this drawback. Additionally, efficient contrast enhancement (i.e., high

relaxivity) and targeted delivery of contrast agents can independently or synergistically realize contrast at even lower dosages.

Endohedral metallofullerenes (EMFs) comprise one class of materials that have shown great promise to enhance both the safety and efficacy of metal-based therapeutic and diagnostic agents. As analogues of the buckminsterfullerenes, EMFs consist of a carbon cage with an even number of carbon atoms and variable symmetry housing metal ions or a metal-based cluster (**Figure 1**).[14,15] To date, various EMFs containing one or two endohedral metal ions ("conventional EMFs") and metal nitride, carbide, oxide, sulfide, acetylide, and cyanide clusters ("clusterfullerenes") have been isolated. The list of metals[14,16,17] and cluster-metal permutations[18] successfully encapsulated (**Figure 1**; note that the focus is on metallofullerenes and does not reflect the wide variety of small molecules lacking metals and single nonmetallic atoms incarcerated by implantation or "molecular surgery"[19,20]) continues to expand. Clusterfullerenes, in particular, are attractive due to the fact that they can often incorporate more of the active metallic species within the carbon cage, though at the cost of reactivity. Of these, trimetallic nitride template (TNT) EMFs are especially promising given their high production yields and stabilities.[21,22] Of particular interest to this feature article are the lanthanide EMFs, with both heavy nuclei, which are advantageous for CT contrast, and excellent magnetic properties, an essential property for MRI contrast agents. The ability to house several Gd^{3+} ions per molecule, enhancing their paramagnetism, makes EMF-based MRI contrast agents attractive compared to most single-Gd^{3+} chelates used commercially. The carbon cage is highly stable and traps the endohedral ions. Additionally, all of the carbon atoms are nominally sp^2-hybridized and can participate in various organic reactions typical of alkenes. Thus, the wide arsenal of organic chemistry can be used for
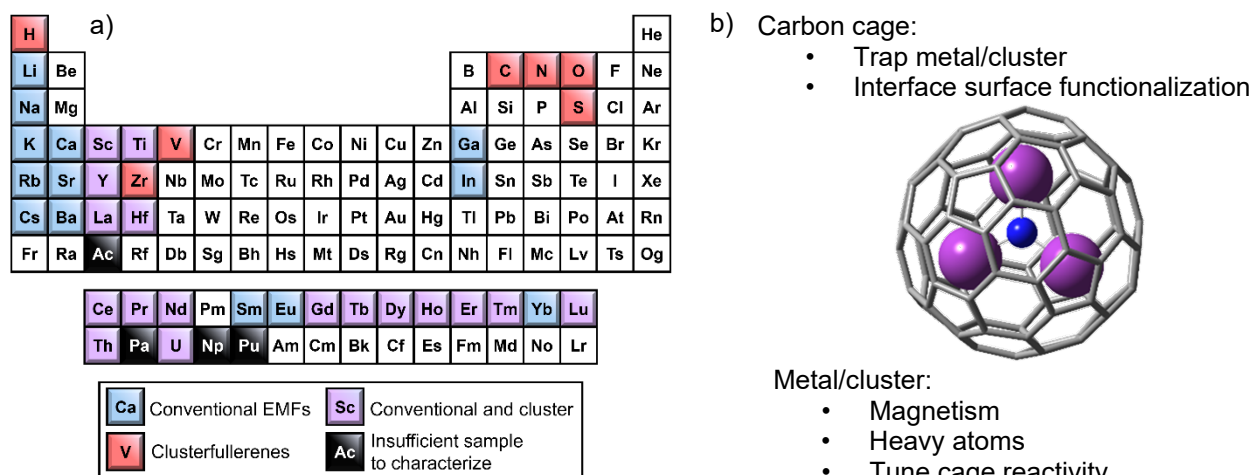
a. Department of Chemistry and Chemical Biology, Rutgers, the State University of New Jersey, 123 Bevier Rd., Piscataway, NJ, 08854
b. Vitale Biotechnology, Inc., 700 West Park Ave., Perkasie, PA, 18944
c. Department of Chemistry, Virginia Polytechnic Institute and State University, 1040 Drillfield Dr., Blacksburg, VA, 24061

Figure 1. (a) The range of elements that have been successfully encapsulated in the indicated variety of EMF by the indicated method(s). Note that species with purely non-metallic endohderal groups are excluded from this figure. (b) A prototypical $M_3N@C_{80}$ TNT EMF, containing an endohedral metal nitride cluster.

functionalization, adding choice ligands to control the solubility, functionality, supramolecular behaviour, and targeting of the EMF.

This feature article will give a brief overview of the relevant chemistry used to take advantage of the unique metal-handling capabilities of EMFs, followed by the development, *in vitro*, and *in vivo* application of EMF derivatives for therapeutic and diagnostic purposes, with a particular emphasis on MRI. Finally, it will discuss recent advances in creating modular, structurally-homogeneous, molecularly-precise derivatives and how this approach can be leveraged for enhanced control over materials properties.

The Chemistry of EMFs

Pristine fullerenes are only soluble in nonpolar solvents, which severely limits their biological applications. Fortunately, the carbon cages can be modified by various methods, which allow their water-soluble derivatives to be prepared.

Generally, water-soluble fullerene derivatives can be obtained by linking C_{60} to polar functional groups covalently or noncovalently. Hydrophilic groups, including carboxyl, hydroxyl, or amino groups, can be covalently attached to C_{60} (**Figure 2**).[23–25] A large number of these small functional groups are often required to bestow water solubility on a fullerene, and the multiadditions are typically not precise or regioselective, yielding mixtures with a heterogeneous number and regiodistribution of functional groups. On the other hand, C_{60} can also form noncovalent complexes with host molecules, such as cyclodextrins, calixarenes, phospholipids, and liposomes.[26–30] In addition to single fullerene molecules, Martín *et al.* constructed a gigantic tridecafullerene with click reactions from a hexakis(malonyl)-derivative of C_{60}, affording a precise multivalent structure with high water solubility and strong anti-viral behavior thanks to its 120 peripheral sugar units.[31] This structure can also achieve higher multivalency with branched ligands.[32]

On the other hand, EMFs are generally less chemically reactive than empty fullerenes, as their cage surfaces are more electron-rich due to electron transfer from the inner metal cluster.[15,33] It is also worth noting that the chemical properties of EMFs are highly dependent on the encapsulated metallic species.[34] Therefore, only a small number of reactions reported for empty fullerenes have been successfully applied to EMFs,[14] among which few regioselective multi-additions have been realized.[35]

Several synthetic methods have been reported to obtain water-soluble EMFs, including treatment with a strong base,[36,37] electrophilic addition,[38,39] nucleophilic reactions,[40,41] radical reactions[42] and multistep Bingel reactions.[43,44] The simplest and most common modification method is polyhydroxylation to yield various metallofullerenols.[45] Among them, extensive studies have been performed on Gd-metallofullerenols. Furthermore, additions of amine,[46] carboxylic acid,[43] glycine esters[40], and amino acids[47,48] to EMFs were also reported.
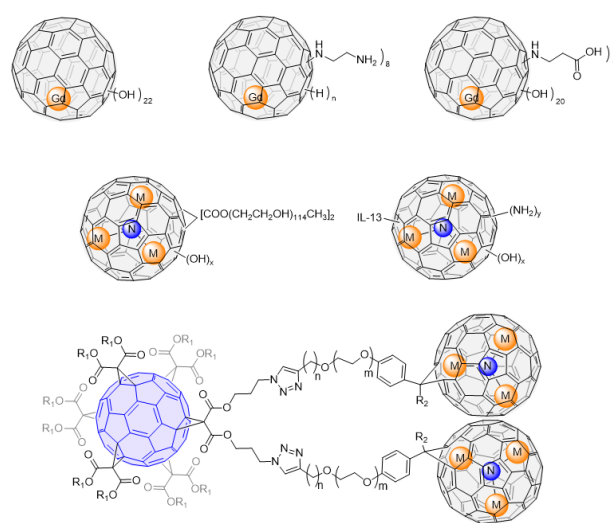
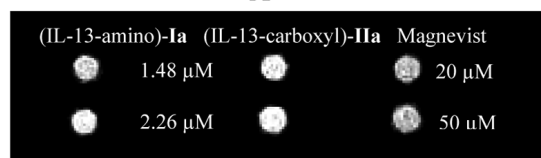**Figure 2.** Representative water-soluble EMF derivatives.

Most synthetic approaches for water-soluble EMF derivatives usually yield mixtures with uncertain addition numbers, a severe obstacle for precise structural design. Recently in 2023, Zhang *et al.* reported the synthesis of the metallobuckytrio (MBT), a three-buckyball system, as a modular platform to develop structurally defined water-soluble EMF derivatives with ligands by choice (*vide infra*).[49]

Biomedical Applications of EMFs

MRI contrast agents

To date, gadolinium-based contrast agents (GBCAs) are the most widely-used contrast agents in MRI examinations. They generate high-contrast images with excellent spatiotemporal resolution, leading to the early detection of various disease conditions *in vivo*.[7] Unfortunately, current commercial GBCAs are Gd chelates, susceptible to *in vivo* leakage of the toxic metal. As mentioned above, Gd leakage from chelation could lead to its accumulation in the brain[12,13] and other parts of the body, causing pathological conditions such as nephrogenic systematic fibrosis.[7,10,11] In contrast, water-soluble derivatives of EMFs, with Gd encapsulated within a robust carbon cage, represent excellent alternatives to traditional GBCAs. Aside from enhanced biosafety, water-soluble EMFs also offer superior relaxivity, as summarized in other reviews[50,51] and as visually demonstrated in **Figure 3**.

As early as 2001, Mikawa *et al.* of the Shinohara group reported that hydroxylated gadofullerenol, $Gd@C_{82}(OH)_n$ possesses almost 20-fold higher relaxivity than commercial contrast agents. The authors demonstrated the distribution of the gadofullerenol contrast agent in the lung, liver, spleen, and kidney of mice after intravenous injection.[36,52] A study by Bolskar *et al.* of the Wilson group demonstrated excellent properties of $Gd@C_{60}[C(COOH)_2]_{10}$ as the first $M@C_{60}$ type EMF derivative for MRI.[43] Fatouros *et al.* reported an *in vivo* study using $Gd_3N@C_{80}[DiPEG5000(OH)_x]$ in mice, demonstrating stronger contrast enhancement compared to intravenous injection of Gd^{3+} chelate.[44] Furthermore, various water-soluble TNT-EMF derivatives, including the carboxylated and hydroxylated derivatives of $Gd_3N@C_{80}$ and ^{177}Lu containing EMF derivatives for radiotherapy, have shown total sealing of the toxic metal cluster inside the fullerene cage, offering protection from potential toxicity.[53–55]

Table 1. Summary of properties of Gd3N@C80[DiPEG(OH)x] MRI contrast agents depicted in **Figure 4**. Adapted with permission from Zhang *et al.*, *Bioconj. Chem.* **2010**, *21*, 610. ©2010, the American Chemical Society.

PEG MW (Da)	Conc. Range (μM)	r_1 (0.35 T) (mM^{-1} s^{-1})	r_1 (2.4 T) (mM^{-1} s^{-1})	r_1 (9.4 T) (mM^{-1} s^{-1})
5000	0.4-6.5	107±8	139±6	52.5±2.4
2000	1.0-15.2	130±4	158±6	41.9±3.0
750	1.1-17.4	152±5	232±10	63.3±1.8
350	1.5-23.5	227±31	237±39	68.2±3.3
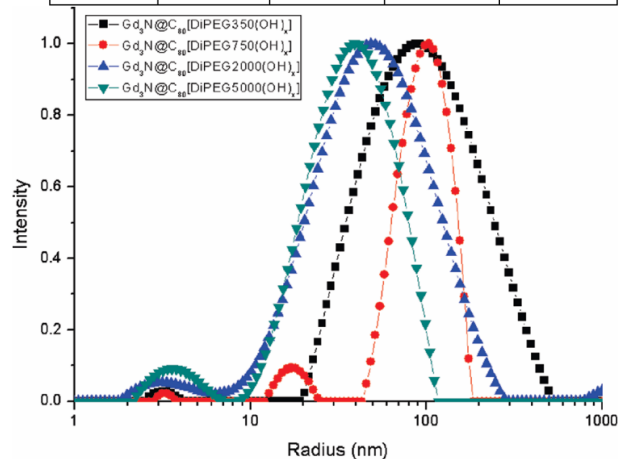
Figure 4. Size distribution of $Gd_3N@C_{80}[DiPEG(OH)x]$ from DLS experiments. The mean peak positions are 75 nm, 76 nm, 58 nm, and 37 nm for $Gd_3N@C_{80}[DiPEG350(OH)x]$, $Gd_3N@C_{80}[DiPEG750(OH)x]$, $Gd_3N@C_{80}[DiPEG2000(OH)x]$ and $Gd_3N@C_{80}[DiPEG5000(OH)x]$, respectively . Reprinted with permission from Zhang *et al.*, *Bioconj. Chem.* **2010**, *21*, 610. ©2010, the American Chemical Society.

Zhang et al. of the Dorn group investigated the effect of aggregation in $Gd_3N@C_{80}[DiPEG]$ systems by altering the length of the polyethylene glycol (PEG) group. Like empty fullerenes, functionalized water-soluble EMF GBCAs bearing hydroxyl, amino, and carboxyl functional groups can dynamically aggregate. The interplay of hydrophobic, hydrophilic, and hydrogen-bonding interactions facilitates such aggregation, as shown in **Figure 4**. The high relaxivity of EMF GBCAs is significantly driven by this aggregation, leading to slower tumbling rates and higher rotational correlation times, as evidenced by the DLS data and corresponding relaxivity measurements (Figure 4). Additionally, the water molecules locked in a hydrogen-bonded network within the aggregate are likely to play an important role in the observed high relaxivity. In the study, longer PEG size caused a reduction in the T_1 relaxivity values by preventing tight aggregation of $Gd_3N@C_{80}$ cages via the hydrogen-bond network from the surface hydroxyl groups. [53]

Figure 3. Inversion– recovery MR images (T1 = 1000 ms, TR = 5000 ms, TE = 30 ms) with IL-13-TAMRA-$Gd_3N@C_{80}O_{~12}(OH)_{~10}(NH_2)_{~7}(NO_2)_2$ ((IL-13-amino)-Ia) and IL-13-TAMRA-$Gd_3N@C_{80}(OH)_{~26}(CH_2CH_2COOM)_{~16}$ ((IL-13-carboxyl)-IIa) and Magnevist as contrast agent. The conjugated nanoparticles exhibit similar contrast with the commercial contrast agent. Reprinted with permission from Li *et al.*, *J. Am. Chem. Soc.* **2015**, *137*, 7881. ©2015, the American Chemical Society.
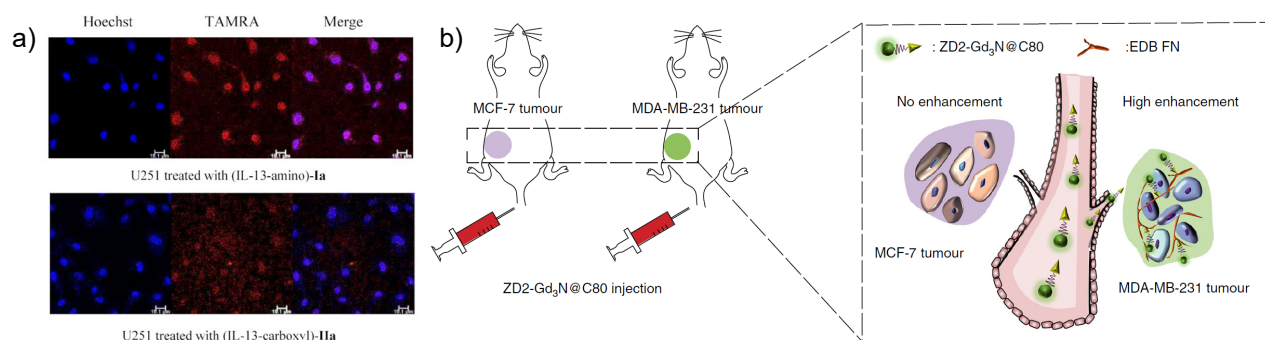
Figure 5. (a) Images are projections of confocal z-stacks, comparing internalization of TAMRA in U-251 cells. Scale bar = 19.1 μm. Top row is U-251 treated with IL-13-TAMRA-Gd$_3$N@C$_{80}$O$_{\sim 12}$(OH)$_{\sim 10}$(NH$_2$)$_{\sim 7}$(NO$_2$)$_2$ ((IL-13-amino)-Ia), and bottom row is U-251 treated with IL-13-TAMRA-Gd$_3$N@C$_{80}$(OH)$_{\sim 26}$(CH$_2$CH$_2$COOH)$_{\sim 16}$ ((IL-13-carboxyl)-IIa). Reprinted with permission from Li *et al.*, *J. Am. Chem. Soc.* **2015**, *137*, 7881. ©2015, the American Chemical Society. (b) Illustration of tumour targeting with ZD2-Gd$_3$N@C$_{80}$ for detection and characterisation of breast cancer in mouse models. MCF-7 and MDA-MB-231 cells were used to obtain low-risk and high-risk breast cancer xenografts, respectively. Reprinted with permission from Han *et al. Nature Commun.* **2017**, *8*, 692 under the Creative Commons CC BY license.

Furthermore, the symmetry of the EMF cage can also affect the relaxivity of GBCAs. In a report by Zhang *et al.* from the Dorn group,[56] the authors demonstrated high relaxivity of a water-soluble egg shaped EMF derivative, Gd$_3$N@C$_{84}$(OH)$_x$. This EMF derivative exhibited higher relaxivity in low, medium and high magnetic field strength when compared to the similarly functionalized Gd$_3$N@C$_{80}$ metallofullerenol. The ellipsoidal shape and the pentalene motif in Gd$_3$N@C$_{84}$ were the key reasons for its different functionalization pattern, aggregation and relaxivity as pointed out by the authors.

In addition to high relaxivity, the local concentration of the GBCAs is critical to diagnose diseases at an early stage, which benefits from high MRI contrast. Therefore, it is imperative to develop specifically-targeted Gd-EMF-based contrast agents. In a study by Li *et al.* of the Dorn group,[57] Gd$_3$N@C$_{80}$ functionalized with amino groups conjugated to an IL-13 had drastically higher accumulation in glioblastoma U251 cells compared to the carboxylate derivative (**Figure 5**). This is due to the stronger interaction of surface receptors on U251 cells with the IL-13 conjugated to the functionalized nanoparticle leading to specific targeting of this conjugate to U251 glioblastoma cells.
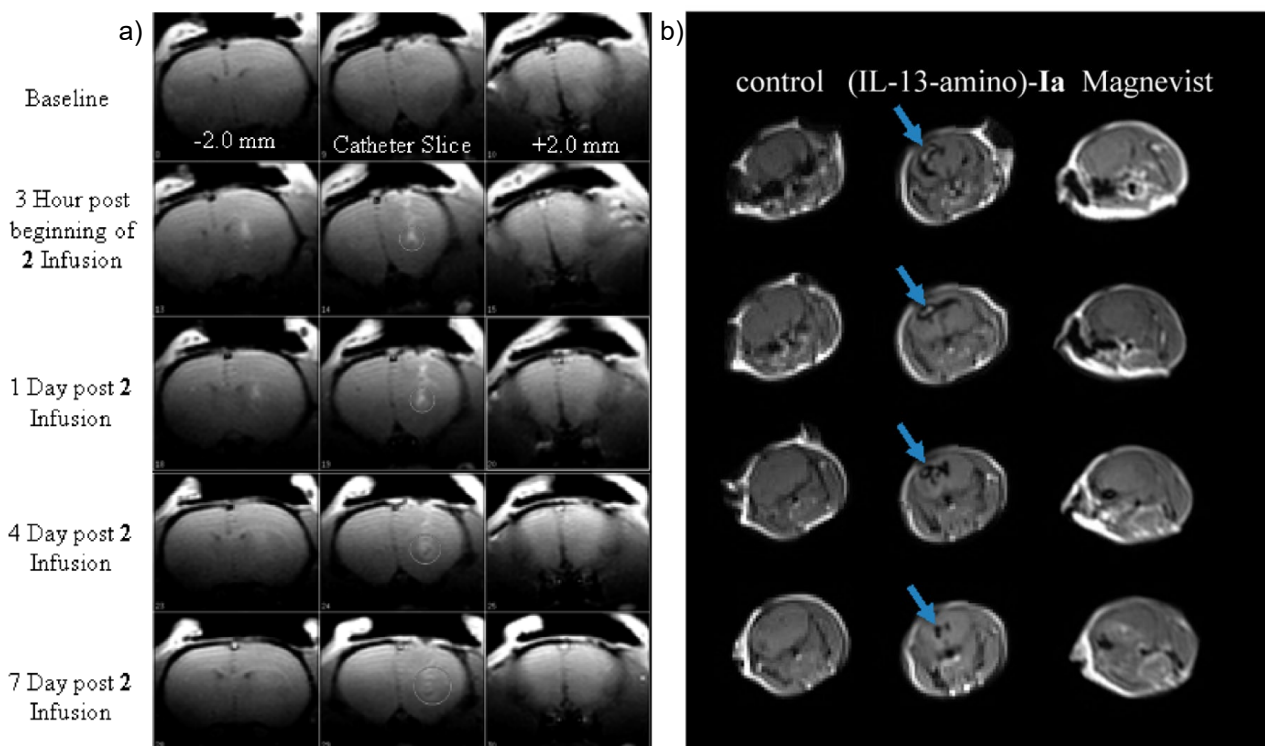
Figure 6. (a) T1 weighted images (TR/TE = 700 ms/10 ms) of direct infusion into T9 tumour-bearing rat brain of 0.0475 mM Gd3N@C$_{80}$(OH)$_{\sim 26}$(CH$_2$CH$_2$COOH)$_{\sim 16}$. Infusion was applied for 120 min at 0.2 μL/min. Reprinted with permission from Shu *et al. Bioconj. Chem.* **2009**, *20*, 1186. ©2009, the American Chemical Society (b) The control image is a mouse brain lacking a tumour. The images labelled (IL-13-amino)-Ia represent MRI of a tumour-bearing mouse brain 15 min after intravenous injection of 300 μL (∼0.9 nmol) of (IL-13-TAMRA-Gd$_3$N@C$_{80}$O$_{\sim 12}$(OH)$_{\sim 10}$(NH$_2$)$_{\sim 7}$(NO$_2$)$_2$. The bright contrast is due to the presence of (IL-13-amino)-Ia. MRI of a tumour-bearing mouse brain after intravenous injection with 100 μL (50 nmol) of commercial contrast agent Magnevist is shown for comparison. Reprinted with permission from Li *et al.*, *J. Am. Chem. Soc.* **2015**, *137*, 7881. ©2015, the American Chemical Society.
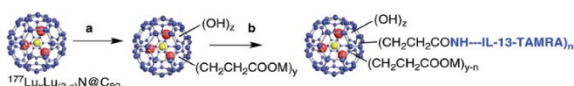
Figure 7. Functionalization and Conjugation of $^{177}Lu_xLu_{3-x}N@C_{80}$ with TAMRA-Labeled IL-13 Peptide ($z \approx 26$, $y \approx 16$, n) 1, 2) used for radiolabeling application. Reprinted with permission from Shultz *et al. J. Am. Chem. Soc.* **2010**, *132*, 4980. ©2010, the American Chemical Society.

In a study by Han *et al.* of the Lu group,[58] a $Gd_3N@C_{80}$ conjugated to a peptide could specifically image extradomain-B fibronectin in triple-negative breast cancer but not in estrogen receptor-positive MCF-7 tumours.

Furthermore, several studies have demonstrated the efficacy of EMF GBCAs (**Figure 6**) *in vivo*. Shu *et al.* of the Dorn group[55] showed the precision and retention advantage of a $Gd_3N@C_{80}$ decorated with carboxylates over Gd chelates. Administered through direct infusion, at a rate of 0.2 µL/min for 120 minutes into a T9-tumour-bearing rat brain, precise tumour detection could still be achieved even 7 days post-injection, as shown in **Figure 6a**. Tthis work demonstrated longer retention (~7 days post-injection) of the contrast agent *in vivo,* which is a clear advantage of gadofullerene-based contrast agents over small-molecule Gd chelates, which are typically cleared within hours. Moreover, $Gd_3N@C_{80}$, functionalized with amino groups, shown in **Figure 6b**, could detect orthotopically implanted U-251 tumour 15 minutes after intravenous injection of 0.9 nmol the nanoparticle, delivering higher contrast than the commercial Gd chelate, Magnevist.[57]

X-Ray contrast agents

Water-soluble EMF derivatives present an appealing alternative to traditional iodinated X-ray contrast agents, which can incite allergic reactions and nephropathy in patients.[59] Additionally, the X-ray attenuation of iodine is inefficient in clinical settings where high-energy X-rays are used. As substitutes, water-soluble EMFs containing different lanthanides such as Dy, Er, and Eu have been tested as X-ray contrast agents.[60] Particularly, Lu-based EMF derivatives exhibit substantial contrast in X-ray images due to the large absorption cross-section of Lu compared to the other lanthanide metals.[61]

Radiotracers

Radiotherapy is a promising therapeutic intervention in medicine, as it can provide localized ionizing radiation with a short penetration range, making it ideal for specific targeted therapy.[62] EMF derivatives containing radionuclides have been used for just this purpose. For example, $^{212}Pb@C_{60}$ derivatized with malonate esters showed promising α-decay results, as reported by Diener *et al.* [62] It was not found to accumulate in the bone as much as current chelated radionuclides, as determined through a biodistribution study holding promise in radiotherapy. In further work by Shultz *et al.* of the Dorn group,[54] ^{177}Lu, a β-emitter, was encapsulated in EMF $Lu_3N@C_{80}$ conjugated to an IL-13 (**Figure 7**). It was found to be confined inside the EMF cage for at least one half-life (6.7 days), showing potential for radiotherapy applications.

Anti-neoplastic activity

Functionalized water-soluble EMF derivatives have also shown great promise in cancer therapy. Although the outcome of the treatment with EMF nanomaterials designed for such a purpose is to cause tumour cell death, the mechanisms of action of various types of derivatives can be very different. As shown in **Figure 8a**, a gadofullerenol, $Gd@C_{82}(OH)_{22}$, could block epithelial-to-mesenchymal (EMT) transition in triple-negative breast cancer cells, inhibiting tumour metastasis.[63] In another report by Lu *et al.*,[64] $Gd@C_{82}$ decorated with alanine was used to induce melanoma cancer tumour cell necrosis. The mechanism of action of these nanoparticles was the destruction of tumour vasculature through the light-assisted generation of $^1O_2$ (**Figure 8b**). Guan *et al.*,[65] reported a similar mechanism when discussing the anti-tumour response of $Gd@C_{82}$ alanine nanoparticles. Additionally, it has been reported that
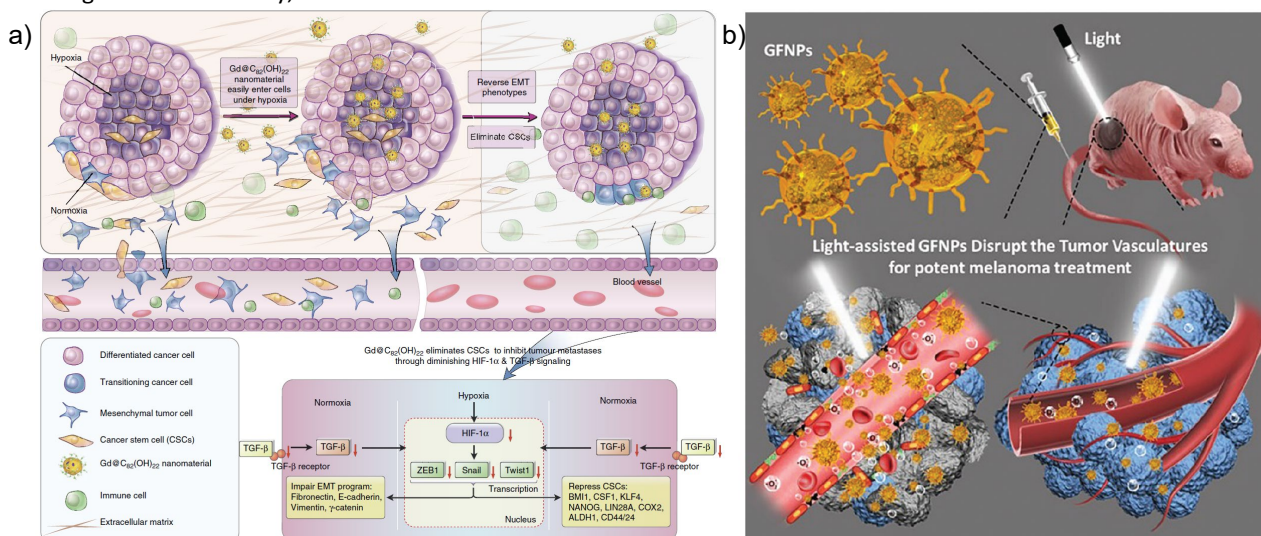
Figure 8. (a) Schematic diagram of key pathways by which $Gd@C_{82}(OH)_{~22}$ nanoparticles inhibits tumour growth. Reprinted with permission from Liu *et al. Nature Commun.* **2015**, *6*, 5988 under the Creative Commons CC BY license. (b) Schematic diagram of light-assisted GFNPs disrupting the tumour vasculatures for potent melanoma treatment. Reprinted with permission from Lu *et al. J. Mater. Chem. B* **2020**, *8*, 2508. ©2020, the Royal Society of Chemistry.
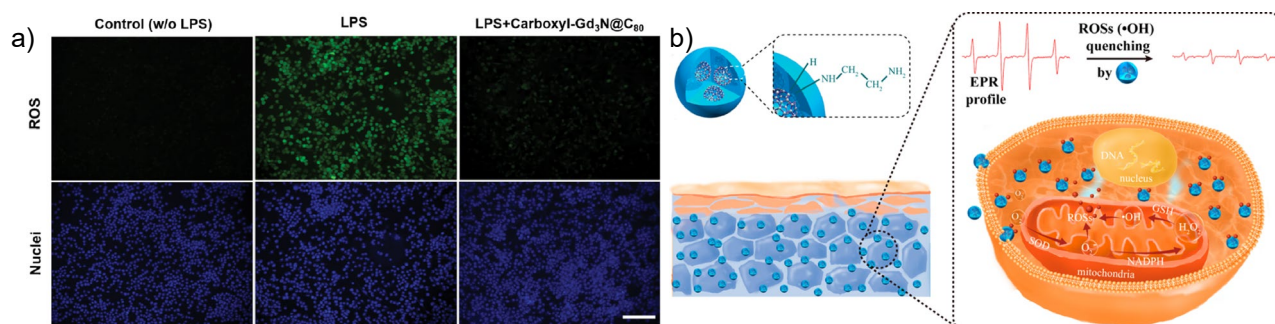
Figure 9. (a) Representative fluorescence images of intracellular ROS illustrating robust ROS-scavenging activity of polycarboxyl-$Gd_3N@C_{80}$. Image taken at ×200 magnification. Scale bar represents 100 μm. Reprinted with permission from Li *et al. ACS Appl. Mater. Interfaces* **2017**, *9*, 17681. ©2017, the American Chemical Society. (b) Schematic diagram of ROS scavenging by $Gd@C_{82}$-(ethylenediamine)$_{-8}$. Reprinted with permission from Li *et al. ACS Appl. Mater. Interfaces* **2016**, *8*, 25770. ©2016, the American Chemical Society.

gadofullerene nanoparticles can undergo a phase transition upon accumulation in tumour blood vessels when exposed to radiofrequency, leading to explosive structural changes and thereby causing tumour necrosis. Several studies have observed this radiofrequency-assisted anti-cancer activity, showing the promise of water-soluble EMF derivatives in cancer therapy.[66–68]
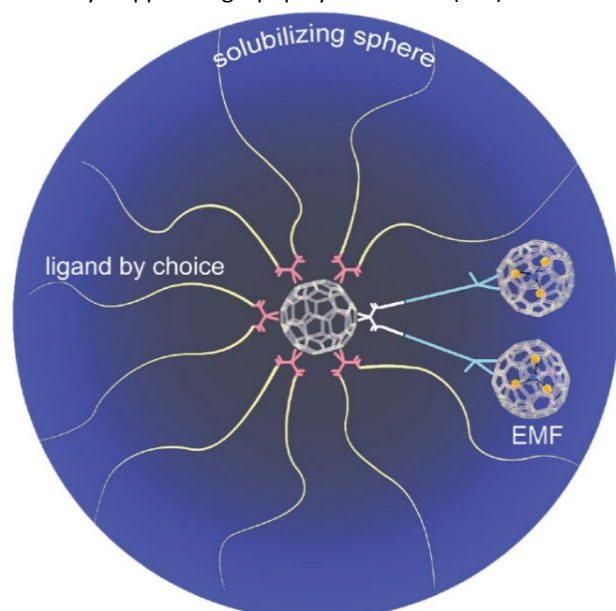
ROS scavenging and anti-inflammatory behaviour

Due to their large, conjugated aromatic cage, EMF derivatives can directly interact with ROS and scavenge reactive radical species, reducing oxidative stress. Several studies have documented this promising behaviour in the context of inflammatory conditions.[69–71] In the work by Li *et al.*,[69] the authors reported that a carboxylate derivative of $Gd_3N@C_{80}$ with radical-scavenging activity was found to exert an anti-inflammatory effect by suppressing lipopolysaccharide (LPS)-elicited mRNA


Figure 10. The general approach for creating water-soluble, molecularly-precise EMF derivatives. Two rounds of CuAAC are used to attach linkers and solubilizing chains in a modular approach. Reprinted with permission from Li *et al. Angew. Chem. Int. Ed.* **2023**, *62*, e202211704 under the Creative Commons CC BY license.

expression of pro-inflammatory enzymes such as Nrf2 and heme oxygenase-1 (**Figure 9a**). Additionally, $Gd@C_{82}$ decorated with ethylenediamine groups (**Figure 9b**) was an excellent ROS scavenger and exhibited cytoprotective effects in HEK-a cells at a low concentration of 2.5 μM. In another work reported by Zhang *et al.*,[72] gadofullerene nanoparticles were able to alleviate oxidative injury after chemotherapy treatment in a mouse model of hepatocarcinoma, which resulted in a prominent increase in blood cells and primary organs.

Multi-EMF Conjugates

Unique among the examples discussed so far are the multi-EMF conjugates produced by the Zhang group.[48] Here, the functional unit is not simply the EMF itself, but two EMFs and a defined number of tailored linkers working in tandem to enable MRI contrast (**Figure 10**). This enables greater control over the molecular structure at the expense of more synthetic steps and effectively decouples the challenges of EMF functionalization and solubilization, opening the door to functional control by adjusting structural parameters. Isomerically-pure $M_3N@C_{80}$ monoadducts were connected to a C_{60} hexakisadduct core, which is a proven strategy to create fullerene cores with a defined and predictable number of substituents.[31,73] For water-soluble MBTs, a combination of one malonate ester and five of another were appended to the surface of the core C_{60} to produce a monoisomeric product (a "[5:1]" motif).[74] This functionalization strategy then enabled the attachment of either two $Lu_3N@C_{80}$ or two $Gd_3N@C_{80}$ EMFs to the first malonate ester, forming a three-buckyball "metallobuckytrio" (MBT) core, that can be purified by flash chromatography, carefully characterized, and stored on shelf for an extended period.[48] In a subsequent step, hydrophilic ligands of one's choosing can be introduced to not only impart water solubility to the final MBT product, but also, if desired, specific biological functionality. In the proof-of-concept work, the initial choice of the hydrophilic ligands were PEG chains of different lengths, but the modular design of the MBT platform can obviously take other ligands of similar sizes to realize multivalent biological interactions.

ChemComm
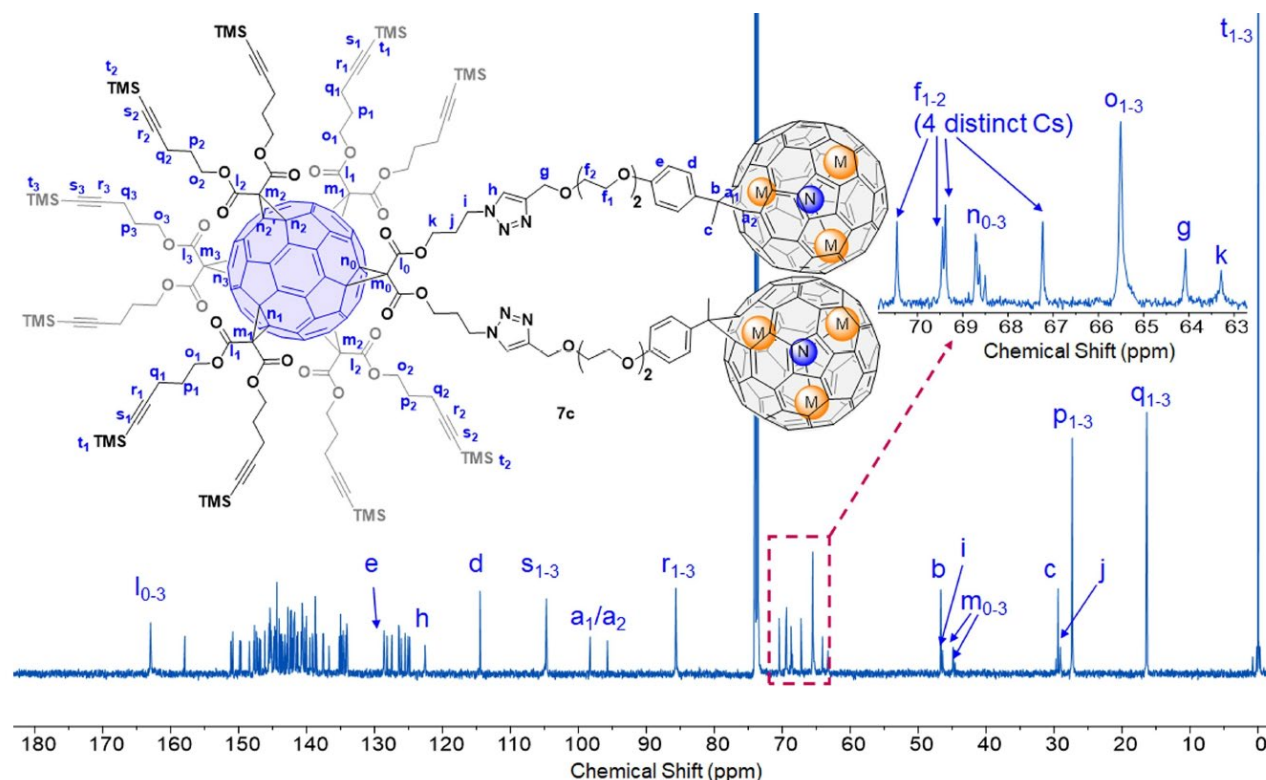
Figure 11. ^{13}C NMR of C_{60} core bearing two $Lu_3N@C_{80}$ EMFs prior to removal of the TMS groups and the second round of CuAAC. A single compound with a single regioisomer is obtained. Reprinted with permission from Li *et al. Angew. Chem. Int. Ed.* **2023**, *62*, e202211704 under the Creative Commons CC BY license.

The level of structural control in water-soluble MBTs relative to their multihydroxyl, -carboxyl, or -amino predecessors is unprecedented. Though complex, one can even get ^{1}H, ^{13}C (**Figure 11**), and 2D NMR spectra of diamagnetic MBT cores , as well as their mass spectra, that attest to the exactness and regioregularity of the products. Building on the robust characterization of the MBT cores, the successful introduction of 10 hydrophilic ligands was confirmed by ^{1}H NMR integration. This exactness brings the opportunity to tune behavioural and property features with clarity and precision. For instance, the mean diameter of supramolecular MBT aggregates in water was shown by dynamic light scattering (DLS) to decrease from ~330

nm to ~250 nm by reducing the linker between the C_{60} core and EMFs from a penta(ethylene glycol) with three methylene units connecting it to the triazole ring to a tri(ethylene glycol) with one methylene. This change likely indirectly impacts EMF-EMF interactions by introducing steric constraints, thereby limiting contact between their large, hydrophobic, aromatic surfaces.

These water-soluble MBTs were confirmed not to release the encapsulated metal ions by ICP-MS with a sub-ppb detection limit. Further, they were shown to be biocompatible in cell viability studies with representative normal (NIH-3T3), cancer (HeLa) and stem cells (iPSC-NSC). All Gd MBTs **8d, 8d'** and **8e** showed high relaxivity compared to typical Gd chelates (**Figure 12**; see **Table 2** for a summary of structural variation). Comparing to **8d**, **8d'** showed a roughly 15% decrease in the r_1 values, with an identical linker between the core and EMF but substantially longer peripheral solubilizing chains. On the other hand, **8d** and **8e** have identical
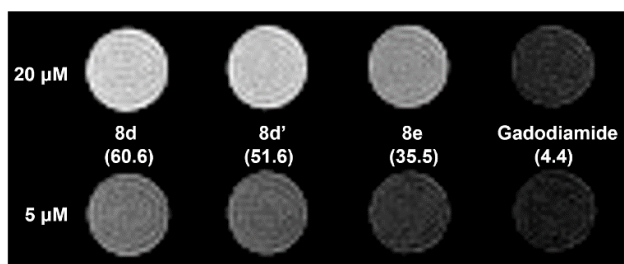
Figure 12. A comparison of MRI contrast images of MBT derivatives with $(CH_2CH_2O)_5(CH_2)_3$ linkers between the core and EMFs and PEG_{12}-Me peripheral solubilizing chains (8d), $(CH_2CH_2O)_5(CH_2)_3$ linkers and PEG1000-Me peripheral solubilizing chains (8d'), and $(CH_2CH_2O)_3CH_2$ linkers and PEG_{12}-Me peripheral solubilizing chains (8e). Commercial MRI contrast agent Gadodiamide is shown at right for comparison. The concentrations of compound used in each series are shown at left. r1 values (mM^{-1} s^{-1}) at 1.4 T magnetic field strength are written in parentheses. Reprinted with permission from Li *et al. Angew. Chem. Int. Ed.* **2023**, *62*, e202211704 under the Creative Commons CC BY license.

Table 2. Structural features of MBT variants discussed in this review. Adapted with permission from Li *et al. Angew. Chem. Int. Ed.* **2023**, *62*, e202211704 under the Creative Commons CC BY license.

MBT Variant	Metal	Linker	Peripheral Chain
8b	Lu	$(CH_2CH_2O)_5(CH_2)_3$	PEG_{12}-Me
8b'	Lu	$(CH_2CH_2O)_5(CH_2)_3$	PEG1000-Me
8c	Lu	$(CH_2CH_2O)_3CH_2$	PEG_{12}-Me
8d	Gd	$(CH_2CH_2O)_5(CH_2)_3$	PEG_{12}-Me
8d'	Gd	$(CH_2CH_2O)_5(CH_2)_3$	PEG1000-Me
8e	Gd	$(CH_2CH_2O)_3CH_2$	PEG_{12}-Me

peripheral solubilizing chains, but the latter has much shorter linkers between the core and EMFs, leading to a 41% decrease in its r_1 value. Overall, structural features bringing more water molecules close to the Gd EMFs would lead to higher relaxivity of the MBTs.

Although the Gd MBTs showed decently high T_1 relaxivity compared Gd chelates, likely due to the large hydrodynamic size of their aggregates, their r_1 values are not as stellar as those metallofullerene derivatives with hydroxyl groups on the cage (especially on per Gd basis) that could exchange protons with water. While the Gd MBT platform is promising for the development of MRI contrast agents, in future ligand design, the improvement of water molecule retention by the ligands should be an important consideration.

Relaxivity of multi-metal metallofullerenes

Relaxivity, the measure of contrast enhancement per unit concentration, is a critical parameter for MRI contrast agents. Although the definition of relaxivity for conventional, chelate-based GBCAs is very clear, it is less straightforward when it comes to EMF GBCAs with more than one Gd^{3+} per EMF, such as $Gd_3N@C_{80}$: when each Gd^{3+} cannot independently leak out the cage, which concentration is more appropriate for relaxivity? The concentration of Gd^{3+} ions, or $Gd_3N@C_{80}$ molecules? This question is more prominent for the MBT system, where one molecule contains 6 Gd^{3+} ions. Taking **8d** for example, while the molecular T_1 relaxivity is 60.6 $mM^{-1}s^{-1}$, it would be 30.3 $mM^{-1}s^{-1}$ based on EMF concentration, or 10.1 $mM^{-1}s^{-1}$ based on Gd^{3+} ion concentration.

To properly answer this question, we should step back and look at why relaxivity is important in the first place. High-relaxivity GBCAs are always desirable because many physiological conditions impose a ceiling for the local concentration of GBCAs, and in a clinical setting, physicians cannot give unlimited amounts of GBCAs to patients. To this end, representing relaxivity properly depends on the context of the discussion or the practical limitations of using higher concentrations. Historically, relaxivity values of trimetallic nitride Gd_3N EMFs were often reported based on molecular concentrations, because each Gd^{3+} cannot independently induce toxicity (unlike Gd^{3+} complexes), and the overall limiting factor is the availability and toxicity of $Gd_3N@C_{2n}$ molecules. On the other hand, relaxivity per Gd can be cited when discussing the influence of chemical environment on relaxivity.[50] In the same vein, for MBTs, the three relaxivity values mentioned above are appropriate in different contexts: when discussing the structural features and chemical environment of the Gd^{3+} ion, relaxivity per Gd is more relevant; when the availability and cost of $Gd_3N@C_{80}$ is practically the limiting factor for its application, then relaxivity per EMF should be used; when the toxicity and molecular local concentration are the limiting factors, then relaxivity per MBT molecule is the most relevant parameter. We note that in the MBT systems, the capacity of incorporating multiple Gd ions in one molecule is an advantage by its own right, akin to the multi-iodine design in CT contrast agents.

Conclusions and Future Direction

Great strides have been made in the safety and efficacy of EMF-based diagnostic and therapeutic agents and their programmability regarding supramolecular behaviour. The propensity for various functional groups to cause EMFs to aggregate in predictable ways based on solubility modification and intermolecular interactions has been established and leveraged for favourable material properties. Modulation of behaviour by control of pH, applied radio waves, light, and the inclusion of targeting moieties have all been successfully employed. In addition, structural control has been achieved through the development of the MBT platform, in which variation in linker lengths directly impacted the observed properties of the studied derivatives. However, there remains a vast range of opportunities for further exploration. Lanthanides capable of operating as T_2 contrast agents, such as Tb, are coming under increasing scrutiny,[75–78] since T_2 contrast agents increase rather than decrease their efficiencies with increasing magnetic field strength.[79] As such, experimenting with Tb EMFs[80,81] could be a promising new avenue for expanding the state of the art in EMF-based MRI contrast agents. Furthermore, in the MBT work described here, two linker lengths and two lengths of peripheral solubilizing chains were investigated for the MBT system, all made of PEG; investigating a wider range of lengths and materials – neutral, cationic, or anionic – could reveal a wider range of available aggregation states and facilitate optimization of r_1 values for MRI contrast agents. Additionally, as shown by the Dorn group, appending targeting groups, such as peptides or polysaccharides, to a functionalized, EMF-based MRI contrast agent is certainly within reach. Combining this approach with the precision afforded by the MBT system could be taken advantage of for a variety of outcomes: targeting combined with optimized r_1 values, multivalent binding to a target for enhanced affinity and low-concentration detection, or combining more than one modality in the same agent. With the global annual production capacity of fullerenes well exceeding 1 metric ton per year, and EMFs comprising ~0.5% of the yield vs. empty-cage fullerenes, placing EMF production well into the kg range, EMFs and their water-soluble derivatives will see a bright future in biomedical applications.

Conflicts of interest

There are no conflicts to declare.

Acknowledgements

References

1 U. Ndagi, N. Mhlongo and M. Soliman, *Drug Des. Devel. Ther.*, 2017, **11**, 599–616.

2   C. X. Zhang and S. J. Lippard, *Curr. Opin. Chem. Biol.*, 2003, **7**, 481–489.

3   B. Seniwal, V. C. Thipe, S. Singh, T. C. F. Fonseca and L. Freitas de Freitas, *Front. Oncol.*, 2021, **11**, 766407.

4   B. M. Yeh, P. F. FitzGerald, P. M. Edic, J. W. Lambert, R. E. Colborn, M. E. Marino, P. M. Evans, J. C. Roberts, Z. J. Wang, M. J. Wong and P. J. Bonitatibus, *Adv. Drug Deliv. Rev.*, 2017, **113**, 201–222.

5   N. Lee, S. H. Choi and T. Hyeon, *Adv. Mater.*, 2013, **25**, 2641–2660.

6   D. V. Hingorani, A. S. Bernstein and M. D. Pagel, *Contrast Media Mol. Imaging*, 2015, **10**, 245–265.

7   J. Wahsner, E. M. Gale, A. Rodríguez-Rodríguez and P. Caravan, *Chem. Rev.*, 2019, **119**, 957–1057.

8   J. Ge, Q. Zhang, J. Zeng, Z. Gu and M. Gao, *Biomaterials*, 2020, **228**, 119553.

9   K. Stockhofe, J. Postema, H. Schieferstein and T. Ross, *Pharmaceuticals*, 2014, **7**, 392–418.

10 P. Marckmann, L. Skov, K. Rossen, A. Dupont, M. B. Damholt, J. G. Heaf and H. S. Thomsen, *J. Am. Soc. Nephrol.*, 2006, **17**, 2359–2362.

11 P. H. Kuo, E. Kanal, A. K. Abu-Alfa and S. E. Cowper, *Radiology*, 2007, **242**, 647–649.

12 T. Kanda, T. Fukusato, M. Matsuda, K. Toyoda, H. Oba, J. Kotoku, T. Haruyama, K. Kitajima and S. Furui, *Radiology*, 2015, **276**, 228–232.

13 R. J. McDonald, J. S. McDonald, D. F. Kallmes, M. E. Jentoft, D. L. Murray, K. R. Thielen, E. E. Williamson and L. J. Eckel, *Radiology*, 2015, **275**, 772–782.

14 A. A. Popov, S. Yang and L. Dunsch, *Chem. Rev.*, 2013, **113**, 5989–6113.

15 A. A. Popov, Ed., *Endohedral Fullerenes: Electron Transfer and Spin*, Springer International Publishing, Cham, 2017.

16 P. Jin, Y. Li, S. Magagula and Z. Chen, *Coord. Chem. Rev.*, 2019, **388**, 406–439.

17 W. Shen, L. Bao and X. Lu, *Chin. J. Chem.*, 2022, **40**, 275–284.

18 H. Zhang, J. Xin, H. Jin, W. Xiang, M. Chen, Y.-R. Yao and S. Yang, *Inorganics*, 2023, **11**, 323.

19 S. Bloodworth and R. J. Whitby, *Commun. Chem.*, 2022, **5**, 121.

20 Y. Li, N. Lou, D. Xu, C. Pan, X. Lu and L. Gan, *Angew. Chem. Int. Ed.*, 2018, **57**, 14144–14148.

21 S. Stevenson, G. Rice, T. Glass, K. Harich, F. Cromer, M. R. Jordan, J. Craft, E. Hadju, R. Bible, M. M. Olmstead, K. Maitra, A. J. Fisher, A. L. Balch and H. C. Dorn, *Nature*, 1999, **401**, 55–57.

22 J. Zhang, S. Stevenson and H. C. Dorn, *Acc. Chem. Res.*, 2013, **46**, 1548–1557.

23 J. Cerar and J. Škerjanc, *J. Phys. Chem. B*, 2003, **107**, 8255–8259.

24 L. Y. Chiang, J. B. Bhonsle, L. Wang, S. F. Shu, T. M. Chang and J. R. Hwu, *Tetrahedron*, 1996, **52**, 4963–4972.

25 C. F. Richardson, D. I. Schuster and S. R. Wilson, *Org. Lett.*, 2000, **2**, 1011–1014.

26 S. Filippone, F. Heimann and A. Rassat, *Chem. Commun.*, 2002, **2002**, 1508–1509.

27 J. L. Atwood, G. A. Koutsantonis and C. L. Raston, *Nature*, 1994, **368**, 229–231.

28 K. C. Hwang and D. Mauzerall, *Nature*, 1993, **361**, 138–140.

29 R. V. Bensasson, E. Bienvenue, M. Dellinger, S. Leach and P. Seta, *J. Phys. Chem.*, 1994, **98**, 3492–3500.

30 C. Ungurenasu and A. Airinei, *J. Med. Chem.*, 2000, **43**, 3186–3188.

31 A. Muñoz, D. Sigwalt, B. M. Illescas, J. Luczkowiak, L. Rodríguez-Pérez, I. Nierengarten, M. Holler, J.-S. Remy, K. Buffet, S. P. Vincent, J. Rojo, R. Delgado, J.-F. Nierengarten and N. Martín, *Nat. Chem.*, 2016, **8**, 50–57.

32 J. Ramos-Soriano, J. J. Reina, B. M. Illescas, N. de la Cruz, L. Rodríguez-Pérez, F. Lasala, J. Rojo, R. Delgado and N. Martín, *J. Am. Chem. Soc.*, 2019, **141**, 15403–15412.

33 J. M. Campanera, C. Bo and J. M. Poblet, *Angew. Chem. Int. Ed.*, 2005, **44**, 7230–7233.

34 X. Lu, L. Feng, T. Akasaka and S. Nagase, *Chem. Soc. Rev.*, 2012, **41**, 7723–7760.

35 Y. Li, Y. Sun, W. P. Kopcha and J. Zhang, *Chin. J. Chem.*, 2023, **41**, 2025–2034.

36 M. Mikawa, H. Kato, M. Okumura, M. Narazaki, Y. Kanazawa, N. Miwa and H. Shinohara, *Bioconjug. Chem.*, 2001, **12**, 510–514.

37 L. Qu, W. Cao, G. Xing, J. Zhang, H. Yuan, J. Tang, Y. Cheng, B. Zhang, Y. Zhao and H. Lei, *J. Alloys Compd.*, 2006, **408–412**, 400–404.

38 L. J. Wilson, D. W. Cagle, T. P. Thrash, S. J. Kennel, S. Mirzadeh, J. Michael Alford and G. J. Ehrhardt, *Coord. Chem. Rev.*, 1999, **190–192**, 199–207.

39 H. Kato, K. Suenaga, M. Mikawa, M. Okumura, N. Miwa, A. Yashiro, H. Fujimura, A. Mizuno, Y. Nishida, K. Kobayashi and H. Shinohara, *Chem. Phys. Lett.*, 2000, **324**, 255–259.

40 X. Lu, X. Zhou, Z. Shi and Z. Gu, *Inorganica Chim. Acta*, 2004, **357**, 2397–2400.

41 C.-Y. Shu, L.-H. Gan, C.-R. Wang, X. Pei and H. Han, *Carbon*, 2006, **44**, 496–500.

42 D. K. MacFarland, K. L. Walker, R. P. Lenk, S. R. Wilson, K. Kumar, C. L. Kepley and J. R. Garbow, *J. Med. Chem.*, 2008, **51**, 3681–3683.

43 R. D. Bolskar, A. F. Benedetto, L. O. Husebo, R. E. Price, E. F. Jackson, S. Wallace, L. J. Wilson and J. M. Alford, *J. Am. Chem. Soc.*, 2003, **125**, 5471–5478.

44 P. P. Fatouros, F. D. Corwin, Z.-J. Chen, W. C. Broaddus, J. L. Tatum, B. Kettenmann, Z. Ge, H. W. Gibson, J. L. Russ and A. P. Leonard, *Radiology*, 2006, **240**, 756–764.

45 S. Zhang, D. Sun, X. Li, F. Pei and S. Liu, *Fuller. Sci. Technol.*, 1997, **5**, 1635–1643.

46 J. Li, M. Guan, T. Wang, M. Zhen, F. Zhao, C. Shu and C. Wang, *ACS Appl. Mater. Interfaces*, 2016, **8**, 25770–25776.

47 Y. Zhou, R. Deng, M. Zhen, J. Li, M. Guan, W. Jia, X. Li, Y. Zhang, T. Yu, T. Zou, Z. Lu, J. Guo, L. Sun, C. Shu and C. Wang, *Biomaterials*, 2017, **133**, 107–118.

48 X. Li, M. Zhen, C. Zhou, R. Deng, T. Yu, Y. Wu, C. Shu, C. Wang and C. Bai, *ACS Nano*, 2019, **13**, 8597–8608.

49 Y. Li, R. Biswas, W. P. Kopcha, T. Dubroca, L. Abella, Y. Sun, R. A. Crichton, C. Rathnam, L. Yang, Y.-W. Yeh, K. Kundu, A. Rodríguez-Fortea, J. M. Poblet, K.-B. Lee, S. Hill and J. Zhang, *Angew. Chem. Int. Ed.*, 2023, **62**, e202211704.

50 A. Rodríguez-Galván, M. Rivera, P. García-López, L. A. Medina and V. A. Basiuk, *J. Cell. Mol. Med.*, 2020, **24**, 3779–3794.

51 T. Li and H. C. Dorn, *Small*, 2017, **13**, 1603152.

52 H. Kato, Y. Kanazawa, M. Okumura, A. Taninaka, T. Yokawa and H. Shinohara, *J. Am. Chem. Soc.*, 2003, **125**, 4391–4397.

53 J. Zhang, P. P. Fatouros, C. Shu, J. Reid, L. S. Owens, T. Cai, H. W. Gibson, G. L. Long, F. D. Corwin, Z.-J. Chen and H. C. Dorn, *Bioconjug. Chem.*, 2010, **21**, 610–615.

54 M. D. Shultz, J. C. Duchamp, J. D. Wilson, C.-Y. Shu, J. Ge, J. Zhang, H. W. Gibson, H. L. Fillmore, J. I. Hirsch, H. C. Dorn and P. P. Fatouros, *J. Am. Chem. Soc.*, 2010, **132**, 4980–4981.

55 C. Shu, F. D. Corwin, J. Zhang, Z. Chen, J. E. Reid, M. Sun, W. Xu, J. H. Sim, C. Wang, P. P. Fatouros, A. R. Esker, H. W. Gibson and H. C. Dorn, *Bioconjug. Chem.*, 2009, **20**, 1186–1193.

56 J. Zhang, Y. Ye, Y. Chen, C. Pregot, T. Li, S. Balasubramaniam, D. B. Hobart, Y. Zhang, S. Wi, R. M. Davis, L. A. Madsen, J. R. Morris, S. M. LaConte, G. T. Yee and H. C. Dorn, *J. Am. Chem. Soc.*, 2014, **136**, 2630–2636.

57 T. Li, S. Murphy, B. Kiselev, K. S. Bakshi, J. Zhang, A. Eltahir, Y. Zhang, Y. Chen, J. Zhu, R. M. Davis, L. A. Madsen, J. R. Morris, D. R. Karolyi, S. M. LaConte, Z. Sheng and H. C. Dorn, *J. Am. Chem. Soc.*, 2015, **137**, 7881–7888.

58 Z. Han, X. Wu, S. Roelle, C. Chen, W. P. Schiemann and Z.-R. Lu, *Nat. Commun.*, 2017, **8**, 692.

59 S.-B. Yu and A. D. Watson, *Chem. Rev.*, 1999, **99**, 2353–2378.

60 A. Miyamoto, H. Okimoto, H. Shinohara and Y. Shibamoto, *Eur. Radiol.*, 2006, **16**, 1050–1053.

61 E. B. Iezzi, J. C. Duchamp, K. R. Fletcher, T. E. Glass and H. C. Dorn, *Nano Lett.*, 2002, **2**, 1187–1190.

62 M. D. Diener, J. M. Alford, S. J. Kennel and S. Mirzadeh, *J. Am. Chem. Soc.*, 2007, **129**, 5131–5138.

63 Y. Liu, C. Chen, P. Qian, X. Lu, B. Sun, X. Zhang, L. Wang, X. Gao, H. Li, Z. Chen, J. Tang, W. Zhang, J. Dong, R. Bai, P. E. Lobie, Q. Wu, S. Liu, H. Zhang, F. Zhao, M. S. Wicha, T. Zhu and Y. Zhao, *Nat. Commun.*, 2015, **6**, 5988.

64 Z. Lu, W. Jia, R. Deng, Y. Zhou, X. Li, T. Yu, M. Zhen and C. Wang, *J. Mater. Chem. B*, 2020, **8**, 2508–2518.

65 M. Guan, Y. Zhou, S. Liu, D. Chen, J. Ge, R. Deng, X. Li, T. Yu, H. Xu, D. Sun, J. Zhao, T. Zou, C. Wang and C. Shu, *Biomaterials*, 2019, **213**, 119218.

66 M. Zhen, C. Shu, J. Li, G. Zhang, T. Wang, Y. Luo, T. Zou, R. Deng, F. Fang, H. Lei, C. Wang and C. Bai, *Sci. China Mater.*, 2015, **58**, 799–810.

67 X. Li, M. Zhen, R. Deng, T. Yu, J. Li, Y. Zhang, T. Zou, Y. Zhou, Z. Lu, M. Guan, H. Xu, C. Shu and C. Wang, *Biomaterials*, 2018, **163**, 142–153.

68 Y. Zhou, R. Deng, M. Zhen, J. Li, M. Guan, W. Jia, X. Li, Y. Zhang, T. Yu, T. Zou, Z. Lu, J. Guo, L. Sun, C. Shu and C. Wang, *Biomaterials*, 2017, **133**, 107–118.

69 T. Li, L. Xiao, J. Yang, M. Ding, Z. Zhou, L. LaConte, L. Jin, H. C. Dorn and X. Li, *ACS Appl. Mater. Interfaces*, 2017, **9**, 17681–17687.

70 L. Xiao, R. Huang, N. Sulimai, R. Yao, B. Manley, P. Xu, R. Felder, L. Jin, H. C. Dorn and X. Li, *ACS Appl. Bio Mater.*, 2022, **5**, 2943–2955.

71 J. Li, M. Guan, T. Wang, M. Zhen, F. Zhao, C. Shu and C. Wang, *ACS Appl. Mater. Interfaces*, 2016, **8**, 25770–25776.

72 Y. Zhang, C. Shu, M. Zhen, J. Li, T. Yu, W. Jia, X. Li, R. Deng, Y. Zhou and C. Wang, *Sci. China Mater.*, 2017, **60**, 866–880.

73 J.-F. Nierengarten, *Chem Commun*, 2017, **53**, 11855–11868.

74 A. Hirsch and O. Vostrowsky, *Eur. J. Org. Chem.*, 2001, **2001**, 829–848.

75 C. Caro, J. M. Paez-Muñoz, A. M. Beltrán, M. Pernia Leal and M. L. García-Martín, *ACS Appl. Nano Mater.*, 2021, **4**, 4199–4207.

76 F. Chen, M. Chen, C. Yang, J. Liu, N. Luo, G. Yang, D. Chen and L. Li, *Phys. Chem. Chem. Phys.*, 2015, **17**, 1189–1196.

77 M. Harris, S. Carron, L. Vander Elst, S. Laurent, R. N. Muller and T. N. Parac-Vogt, *Chem. Commun.*, 2015, **51**, 2984–2986.

78 R. Zairov, A. Mustafina, N. Shamsutdinova, I. Nizameev, B. Moreira, S. Sudakova, S. Podyachev, A. Fattakhova, G. Safina, I. Lundstrom, A. Gubaidullin and A. Vomiero, *Sci. Rep.*, 2017, **7**, 40486.

79 S. Marasini, H. Yue, S. L. Ho, K.-H. Jung, J. A. Park, H. Cha, A. Ghazanfari, M. Y. Ahmad, S. Liu, Y. J. Jang, X. Miao, K.-S. Chae, Y. Chang and G. H. Lee, *Eur. J. Inorg. Chem.*, 2019, **2019**, 3832–3839.

80 M. Wolf, K.-H. Müller, D. Eckert, Y. Skourski, P. Georgi, R. Marczak, M. Krause and L. Dunsch, *Proc. Jt. Eur. Magn. Symp. JEMS 04*, 2005, **290–291**, 290–293.

81 T. Zuo, C. M. Beavers, J. C. Duchamp, A. Campbell, H. C. Dorn, M. M. Olmstead and A. L. Balch, *J. Am. Chem. Soc.*, 2007, **129**, 2035–2043.